The C-terminus SH3-binding domain of Kv1.3 is required for the actin-mediated immobilization of the channel via cortactin

Peter Hajdu[a,b], Geoffrey V. Martin[a], Ameet A. Chimote[a], Orsolya Szilagyi[a,b], Koichi Takimoto[c], and Laura Conforti[a]

[a]Division of Nephrology and Hypertension, Department of Internal Medicine, University of Cincinnati, Cincinnati, OH 45267; [b]Department of Biophysics and Cell Biology, University of Debrecen, 4032 Debrecen, Hungary; [c]Department of Bioengineering and Bioinformatics, Nagaoka University of Technology, Nagaoka 940-2137, Japan

ABSTRACT **Kv1.3 channels play a pivotal role in the activation and migration of T-lymphocytes. These functions are accompanied by the channels' polarization, which is essential for associated downstream events. However, the mechanisms that govern the membrane movement of Kv1.3 channels remain unclear. F-actin polymerization occurs concomitantly to channel polarization, implicating the actin cytoskeleton in this process. Here we show that cortactin, a factor initiating the actin network, controls the membrane mobilization of Kv1.3 channels. FRAP with EGFP-tagged Kv1.3 channels demonstrates that knocking down cortactin decreases the actin-based immobilization of the channels. Using various deletion and mutation constructs, we show that the SH3 motif of Kv1.3 mediates the channel immobilization. Proximity ligation assays indicate that deletion or mutation of the SH3 motif also disrupts interaction of the channel with cortactin. In T-lymphocytes, the interaction between HS1 (the cortactin homologue) and Kv1.3 occurs at the immune synapse and requires the channel's C-terminal domain. These results show that actin dynamics regulates the membrane motility of Kv1.3 channels. They also provide evidence that the SH3 motif of the channel and cortactin plays key roles in this process.**

Monitoring Editor
Kozo Kaibuchi
Nagoya University

Received: Jul 8, 2014
Revised: Jan 27, 2015
Accepted: Feb 20, 2015

INTRODUCTION

The ability of membrane proteins to compartmentalize in specific membrane domains is essential to cell function. This is particularly true for T-lymphocytes, which polarize when they migrate and activate. Activation of T-lymphocytes is initiated by the encounter with antigen-presenting cells (APCs). The physical interaction between the T-cell and the APC leads to a cascade of cellular events, including polarization of the T-cell, with accumulation of cell surface proteins, intracellular organelles, and signaling molecules at the T-APC contact site, forming a highly organized signaling zone known as the immunological synapse (IS; Cahalan and Chandy, 2009; Kummerow *et al.*, 2009). The movement of specific cell surface proteins into the IS is necessary for proper activation of the T-cell, as disruption of the IS architecture can lead to either T-cell hypoactivation or hyperactivation (Mossman *et al.*, 2005).

One important cell surface protein that localizes to the IS during T-cell activation is the voltage-gated potassium channel, Kv1.3. Kv1.3 channels play an essential role in the T-cell activation process by regulating the electrochemical driving force for Ca^{2+} influx and generation of the intracellular Ca^{2+} concentration ($[Ca^{2+}]_i$) necessary for downstream transcription factor activation and T-cell clonal expansion (Wulff *et al.*, 2003; Hu *et al.*, 2013). Indeed, blocking the Kv1.3 channel current suppresses Ca^{2+} influx and T-cell activation (Cahalan and Chandy, 2009; Hajdu *et al.*, 2013). Furthermore, improper localization of Kv1.3 to the IS leads to altered $[Ca^{2+}]_i$ dynamics and has

This article was published online ahead of print in MBoC in Press (http://www.molbiolcell.org/cgi/doi/10.1091/mbc.E14-07-1195) on March 4, 2015.

The authors affirm that there are no known conflicts of interest associated with this publication and there has been no significant financial support for this work that could have influenced its outcome.

Address correspondence to: Laura Conforti (laura.conforti@uc.edu).

Abbreviations used: APC, antigen-presenting cell; CD, cluster of differentiation; EGFP, enhanced green fluorescent protein; FRAP, fluorescence recovery after photobleaching; hDlg1, human Discs Large homologue 1; HEK-293, human embryonic kidney cell line 293; HEPES, 4-(2-hydroxyethyl)-1-piperazineethanesulfonic acid; HS1, hematopoietic lineage cell-specific protein; PLA, proximity ligation assay; PSD-95, postsynaptic density protein 95; SH3, SRC homology 3; shRNA, short hairpin RNA.

been associated with aberrant T-cell signaling in systemic lupus erythematosus (Nicolaou *et al.*, 2007, 2009, 2010). The exact mechanisms governing the movement of Kv1.3 to the IS and the channel's accumulation at this site are not fully understood, although it has been shown that membrane-incorporated Kv1.3 proteins move into the IS via lateral movement along the plane of the plasma membrane (Nicolaou *et al.*, 2009). The processes by which proteins gather at the IS are in general poorly understood. Synapse organization has often been said to involve the phenomenon of "diffusion trapping," which depends on both passive (molecular diffusion) and active mechanisms (involving the actin cytoskeleton; Favier *et al.*, 2001; Douglass and Vale, 2005; Davis and van der Merwe, 2006; Dushek *et al.*, 2008). The actin cytoskeleton has been implicated in the transport and trapping at the IS of various proteins, including the T-cell receptor (TCR; Dustin, 2007; Dushek *et al.*, 2008; Babich *et al.*, 2012). Several studies reported that association of channels of the Kv1 family with actin is guaranteed by adaptor proteins that possess actin-binding domains: PDZ-binding proteins, such as human Discs Large homologue 1 (hDlg1), and cortactin. The binding of cortactin and PDZ proteins to Kv channels occurs at the C-terminal region of the channel, with cortactin binding associated with a 19–amino acid sequence in Kv1.2 channels and PDZ binding occurring at a TDV amino acid motif in Kv1.3 and Kv1.4 channels (Imamura *et al.*, 2002; Marks and Fadool, 2007; Doczi *et al.*, 2011). In addition, the Src homology 3 (SH3) domain, which can be found on cortactin, PDZ proteins, and Kv channels, may also play a role in these proteins' interactions, as SH3-binding domains have been found to be integral in PDZ protein–induced clustering of Kv1.4 and have been associated with modulation of Kv1.3 current (Shin *et al.*, 2000; Marks and Fadool, 2007). T-cells express the cortactin analogue hematopoietic lineage cell-specific protein 1 (HS1) and the PDZ-binding proteins hDlg1 and postsynaptic density protein 95 (PSD-95), which are able to form complexes with actin and bind multiple Kv channel isoforms (Daly, 2004; Xavier *et al.*, 2004; Carrizosa *et al.*, 2009). HS1 in T-cells was shown to be necessary for the accumulation of F-actin to the IS and the development of the appropriate signaling post IS formation (Gomez *et al.*, 2006). Furthermore, C-terminal truncation of Kv1.3 or knockdown of PSD-95 in Jurkat T-cells has been recently reported to decrease the amount of Kv1.3 channels in the IS at early time points (Szilagyi *et al.*, 2013). Thus, it is possible that the interaction with actin drives and stabilizes Kv1.3 compartmentalization to the IS. Nevertheless, the involvement of the aforementioned proteins in actin-mediated Kv1.3 membrane motility remains unclear. In the present study, we investigated wild-type Kv1.3 channels and C-terminal mutated Kv1.3 channels lacking cortactin-, SH3-, or PDZ-binding motif to further elucidate the mechanisms and the molecular requirements for Kv1.3 lateral membrane mobility and localization.

RESULTS

Colocalization of Kv1.3 channels with cortactin

Cortactin has a Kv channel–binding sequence and binds to various ion channels (Hattan *et al.*, 2002; Tian *et al.*, 2006; Williams *et al.*, 2007; Cheng *et al.*, 2011; Ilatovskaya *et al.*, 2011; Herrmann *et al.*, 2012). Thus, to reveal whether Kv1.3 channels colocalize with cortactin, we performed immunocytochemistry experiments using human embryonic kidney cell line 293 (HEK-293), which stably expresses FLAG-Kv1.3 channels. We labeled the plasma membrane–localized Kv1.3 channels on fixed but nonpermeabilized cells, followed by the intracellular staining of cortactin. Confocal images shown in Figure 1 revealed that the fluorescence signals of labeled membrane Kv1.3 channels (green) and cortactin (red) are highly overlapping, which indicates that these proteins exist in close proximity to each other and predicts a possible interaction between them.

Cortactin/SH3/PDZ-binding-site mutants of Kv1.3

Because confocal images suggested a possible association between Kv1.3 and cortactin, we compared the C-terminal end of Kv1.2 to that of Kv1.3 to determine whether the cortactin- binding sequence identified in Kv1.2 was also present in Kv1.3 (Hattan *et al.*, 2002). A similar 19–amino acid domain was identified in Kv1.3 (Figure 2A). Moreover, SH3-binding (PxxP) and PDZ-binding (FTDV) motifs are also positioned on the C-terminal of Kv1.3 downstream of the putative cortactin-binding site (Figure 2B). On the basis of this analysis, we designed several mutants of Kv1.3 with altered C-terminus. Sequential truncation of the C-terminus resulted in constructs without any recognition sites (putative cortactin, SH3, PDZ: Δ1), with only a putative cortactin-binding motif (Δ2; for the sake of clarity, from now on, "putative cortactin-binding" is defined as simply "cortactin-binding") and a cortactin- and SH3-binding domain (Δ3). With mutation of a few amino acids, we obtained full-length Kv1.3 channels without the SH3-binding domain (ΔSH3) or PDZ-binding sequence (ΔPDZ; Figure 2C). A previously designed C-terminal-truncated mutant, ΔC, was also used (Szilagyi *et al.*, 2013). The effective neutralization of the SH3 domain in this Kv1.3 construct was previously confirmed (Marks and Fadool, 2007). The inability of the ΔPDZ Kv1.3 mutant to bind PDZ proteins was established by immunoprecipitation (Supplemental Figure S1). Cells were cotransfected with myc-Dlg1 and either enhanced green fluorescent protein (EGFP)–tagged wild-type (WT) or ΔPDZ Kv1.3 clones. After immunoprecipitation of Dlg1, Kv1.3 was detected only in cells transfected with WT Kv1.3. All these mutants can thus be used to obtain information on the site of

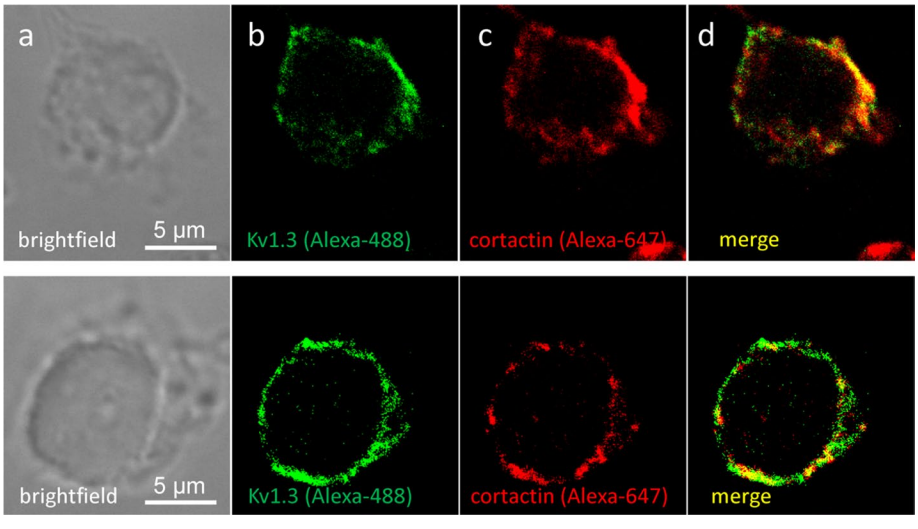

FIGURE 1: Kv1.3 channels colocalize with cortactin. Confocal images of 1-µm thickness of two representative FLAG-Kv1.3–expressing HEK-293 cells labeled with FLAG and cortactin antibodies. (a) Bright-field image of the cell. (b) Kv1.3 (green). (c) Cortactin (red). (d) Overlay of red and green channels. Note that overlapping of the red and the green signals turns yellow, which indicates colocalization. Representative of three independent experiments.

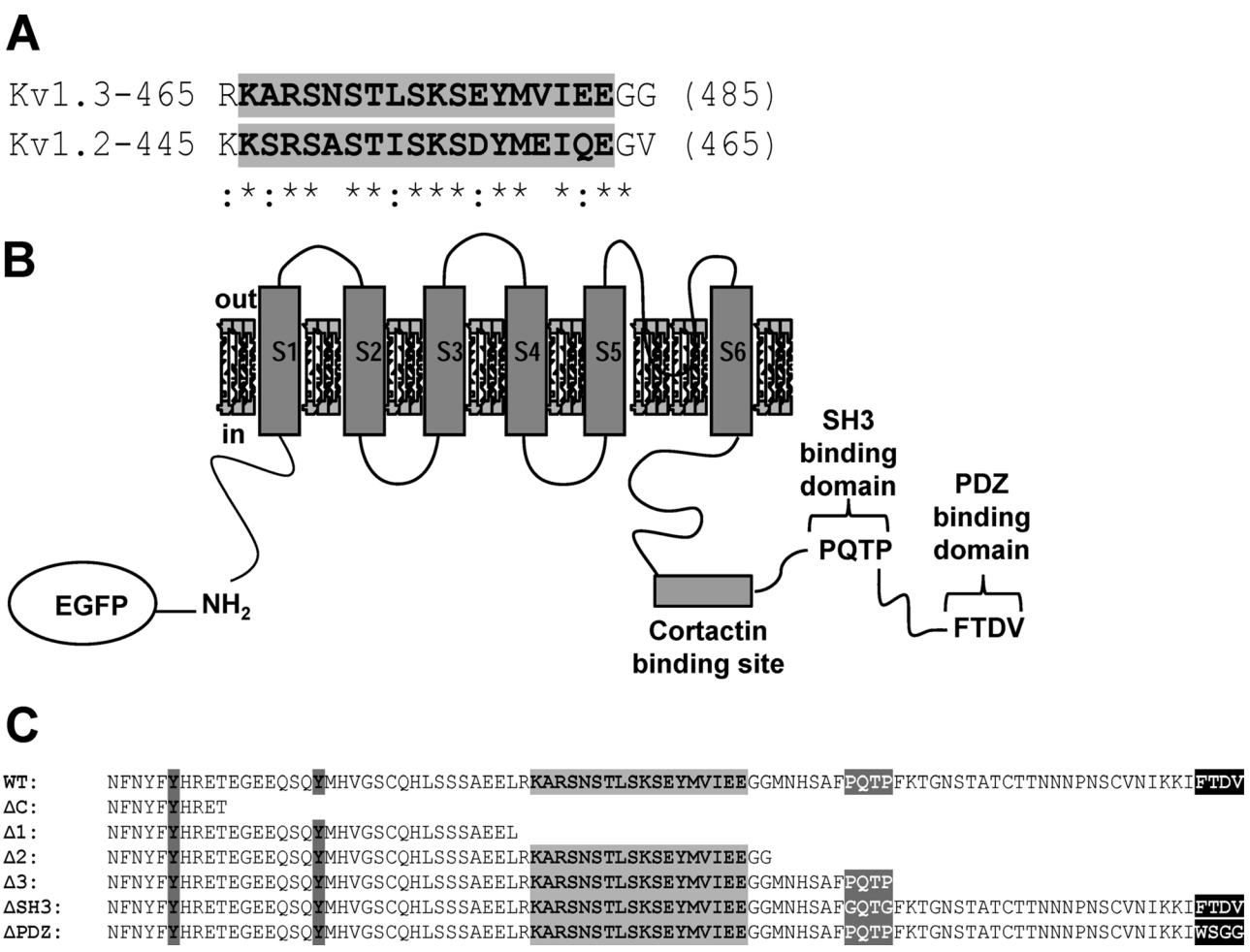

FIGURE 2: Scheme of WT Kv1.3 channel and C-terminal mutations. (A) Alignment of Kv1.2 cortactin-binding site to Kv1.3 C-terminus. (B) Schematic representation of WT Kv1.3 pore-forming α subunit with EGFP tag and cortactin-, SH3-, and PDZ-binding regions. (C) Amino acid sequences of WT Kv1.3 and mutant Kv1.3 C-termini starting at amino acid 431. ΔC truncation removes the entire C-terminus except the HRET sequence, which is needed for membrane targeting. Δ1 mutation represents truncation of Kv1.3 C-terminus before the predicted cortactin-binding site. Δ2 mutant represents truncation of Kv1.3 C-terminus directly after the putative cortactin-binding site. Δ3 mutant represents mutation of Kv1.3 C-terminus directly after the SH3-binding site. ΔSH3 mutant represents an amino acid sequence change from PQTP to GQTG. ΔPDZ mutant represents an amino acid sequence change from FTDV to WSGG. Amino acids are listed by their one-letter designations.

Kv1.3 interaction with cortactin and clarify whether other adaptor proteins (hDlg1, PSD95) are required for this linkage.

Electrophysiology of mutant channels

The deletion of the C-terminus of Kv1.x channels may lead to loss of function and inappropriate sorting of the proteins (Zhu *et al.*, 2003, 2007). Consequently, electrophysiological experiments were performed to verify the appropriate membrane targeting and assembly of each Kv1.3 mutant channel. Kv1.3 variants were transiently transfected into HEK-293 cells, and K^+ currents were recorded in outside-out patches from cells expressing EGFP-tagged channels. Kinetic and equilibrium parameters of Kv1.3 channel's gating for Δ1, Δ2, Δ3, ΔSH3, and ΔPDZ mutants and WT constructs were compared. The biophysical properties of ΔC were determined previously (Szilagyi *et al.*, 2013). No differences were found between ΔC and WT Kv1.3 (Szilagyi *et al.*, 2013). As shown in Figure 3A, the current traces obtained upon a 2-s-long depolarization from a patch expressing WT and Δ1 plasmids are almost identical (not all mutants are shown, for clearer visibility). To obtain time-constant characteristics for inactivation, the declining part of the current trace was fitted with a one-exponential function (see *Materials and Methods*). Figure 3B demonstrates that none of the mutations introduced into Kv1.3 protein modifies the time constant of inactivation (τ_i), which was as follows (in milliseconds): WT, 219 ± 22 (n = 8); Δ1, 233 ± 36 (n = 5); Δ2, 244 ± 33 (n = 7); Δ3, 249 ± 20 (n = 8); ΔSH3, 257 ± 22 (n = 8); and ΔPDZ, 211 ± 34 (n = 11; p = 0.831). Afterward, the steady-state parameters of the voltage dependence of activation, which describes the opening probability of the channel at a certain membrane potential, were determined for all channel constructs: normalized whole-cell conductance was plotted against test potential, and Boltzmann functions were fitted to the data points (only shown for WT and Δ1 in Figure 3C). We found that half-maximal activation voltage ($V_{1/2}$) and slope factor (k) were not statistically different for any mutants of Kv1.3. k was as follows: WT, 12.2 ± 1.2 mV (n = 5); Δ1, 10.1 ± 1 mV (n = 4); Δ2, 11.3 ± 1.1 mV (n = 6); Δ3, 11.6 ± 0.4 mV (n = 6); ΔSH3, 10.6 ± 0.4 mV (n = 5); and ΔPDZ, 13.2 ± 1.2 mV (n = 7; p = 0.285). $V_{1/2}$ was as follows: WT, –20.8 ± 3.5 mV (n = 5); Δ1, –22.0 ± 2.4 mV

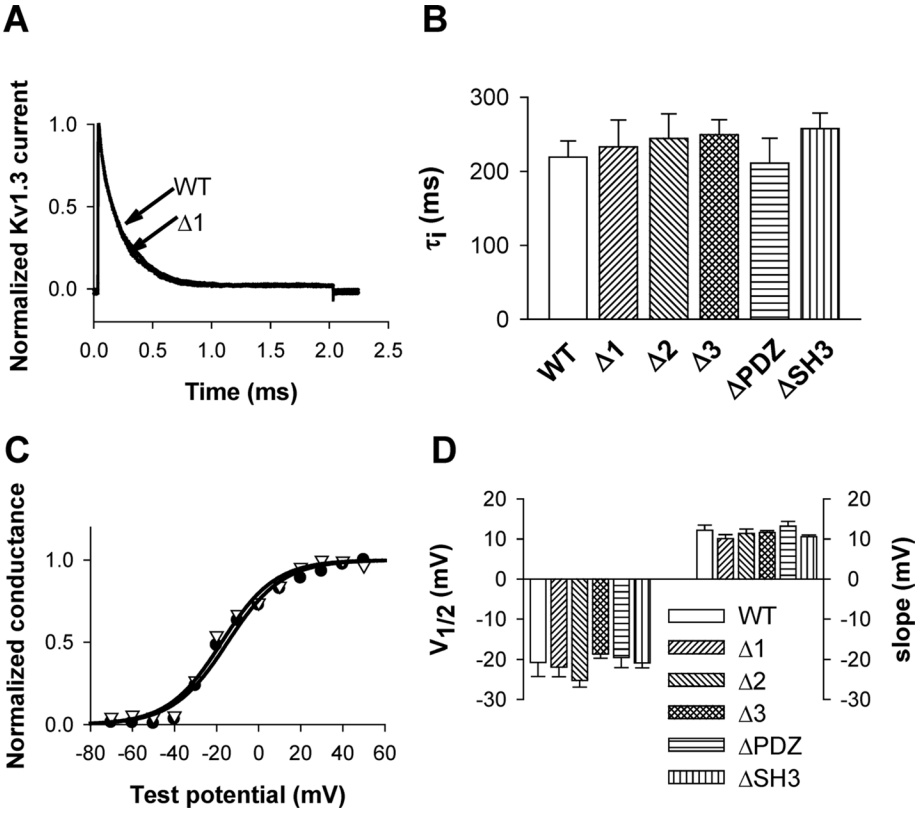

FIGURE 3: Biophysical characterization of Kv1.3 constructs. (A) To determine the inactivation kinetics of the currents, outside-out patches were depolarized to +40 mV for 2 s from a HP of −120 mV. Typical current records for the EGFP-tagged WT and Δ1 construct. (B) Average inactivation time constant (τ_i) for various Kv1.3 mutants. (C) Voltage dependence of steady-state activation of the Kv1.3 channels in HEK-293 cells, outside-out configuration. The normalized conductance–test potential relationships were recorded and evaluated as detailed in *Materials and Methods*. Normalized conductance as a function of the test potential for WT (filled circles) and Δ1 (empty triangles) along with fitted Boltzmann function (solid lines) are plotted for two actual patches. (D) Parameters of steady-state activation (slope, *k*, and midpoint, $V_{1/2}$) are shown for all constructs. The data in B and D are reported as mean ± SEM of 5–11 cells.

($n = 4$); Δ2, −25.2 ± 1.6 mV ($n = 6$); Δ3, −18.7 ± 1.1 mV ($n = 6$); ΔSH3, −20.9 ± 1.1 mV ($n = 5$); and ΔPDZ, −19.6 ± 2.5 mV ($n = 7$; $p = 0.32$, Figure 3D). Consequently, the truncations and amino acid replacements did not modify the biophysical characteristics of the channels.

Interaction of Kv1.3 with cortactin

We used proximity ligation assay (PLA) to learn whether cortactin and Kv1.3 channels interact in HEK-293 cells and which portion of the channel protein is important for this association. This method enables detection of the interaction between proteins that reside at <40-nm distance through species-specific secondary antibodies, each with unique short oligonucleotides, and a polymerase that amplifies the circular DNA that is formed by hybridization when the two antibodies are in close proximity (Soderberg *et al.*, 2006). The GFP antibody, which recognizes the EGFP moiety at the N-terminus of the Kv1.3 channels, was used along with the cortactin antibody. As shown in Figure 4A, HEK-293 cells expressing wild-type EGFP-Kv1.3 clone display positivity for PLA signal: red dots. The same experiments were performed for cells transfected with Δ1, Δ2, Δ3, and ΔSH3 Kv1.3 mutants. Confocal images were analyzed for number of dots, and the results are summarized in Figure 4B. The number of dots/cell in WT Kv1.3 is significantly different from that in all of the Kv1.3 mutants ($p < 0.001$). Furthermore, the PLA signal in the Δ3 mutant is significantly higher than that in Δ1, Δ2, and ΔSH3 mutants ($p < 0.001$). These findings suggest that cortactin binds Kv1.3 in intact cells and that the association between these proteins occurs through the SH3-binding domain. Further PLA experiments confirmed the close proximity and interaction of cortactin with actin, thus suggesting a role for cortactin in linking Kv1.3 to the actin cytoskeleton (Figure 4C; Daly, 2004). We then tested whether the lateral membrane motility of Kv1.3 depends on an active process that is mediated by actin and whether cortactin guarantees the association between Kv1.3 and actin.

Lateral mobility of Kv1.3 channel constructs

The lateral membrane motility of Kv1.3 and its dependence on the actin cytoskeleton and cortactin were established in fluorescence recovery after photobleaching (FRAP) experiments. The recovery of fluorescence in the plasma membrane after photobleaching occurred by lateral membrane diffusion for all transfected Kv1.3 channels, as can be seen by the time series of Kv1.3 fluorescence recovery depicted in Figure 5A and, for WT Kv1.3, in Supplemental Movie S1. Analysis of FRAP recovery curves yielded an estimate of the mobile fraction (M_f) of Kv1.3 channels (Figure 5, A and B). Alterations of Kv1.3 membrane mobility by actin polymerization were determined to establish the role that actin has in the channel motility. Where indicated, jasplakinolide, which is a cyclical peptide of *Jaspis johnstoni* (a marine sponge), was applied for 50 min before FRAP experiments to induce actin polymerization and stabilization of the filaments (Bubb *et al.*, 1994, 2000). The addition of jasplakinolide caused a significant reduction in M_f in the WT and Δ3 and ΔPDZ mutants of 40–50% compared with cells that were not pretreated with jasplakinolide, but jasplakinolide did not affect the M_f of Δ1, Δ2, and ΔSH3 mutants (Figure 5). The average M_f of all channel mutants without jasplakinolide pretreatment was 0.71 ± 0.01 ($n = 41$; Figure 5B). The average M_f of WT, Δ3, and ΔPDZ channels treated with jasplakinolide was 0.43 ± 0.01 ($n = 18$), whereas the average M_f of Δ1, Δ2, and ΔSH3 channels treated with jasplakinolide was 0.63 ± 0.01 ($n = 15$). These outcomes support the importance of the SH3-binding domain in the functional interaction between the channel and actin cytoskeleton.

Role of cortactin in Kv1.3 mobility

FRAP experiments with mutant channels confirmed that cortactin and actin have a role in Kv1.3 channel immobilization. Hence we used another approach to test the role of cortactin: a HEK-293 cell line with depleted cortactin level was established using lentiviral short hairpin RNA (shRNA) transduction. Figure 6A shows that cortactin expression was significantly reduced in cortactin-shRNA virus particle–infected cells (control was nontarget/scramble shRNA–transduced cells). As a next step, we expressed EGFP-tagged

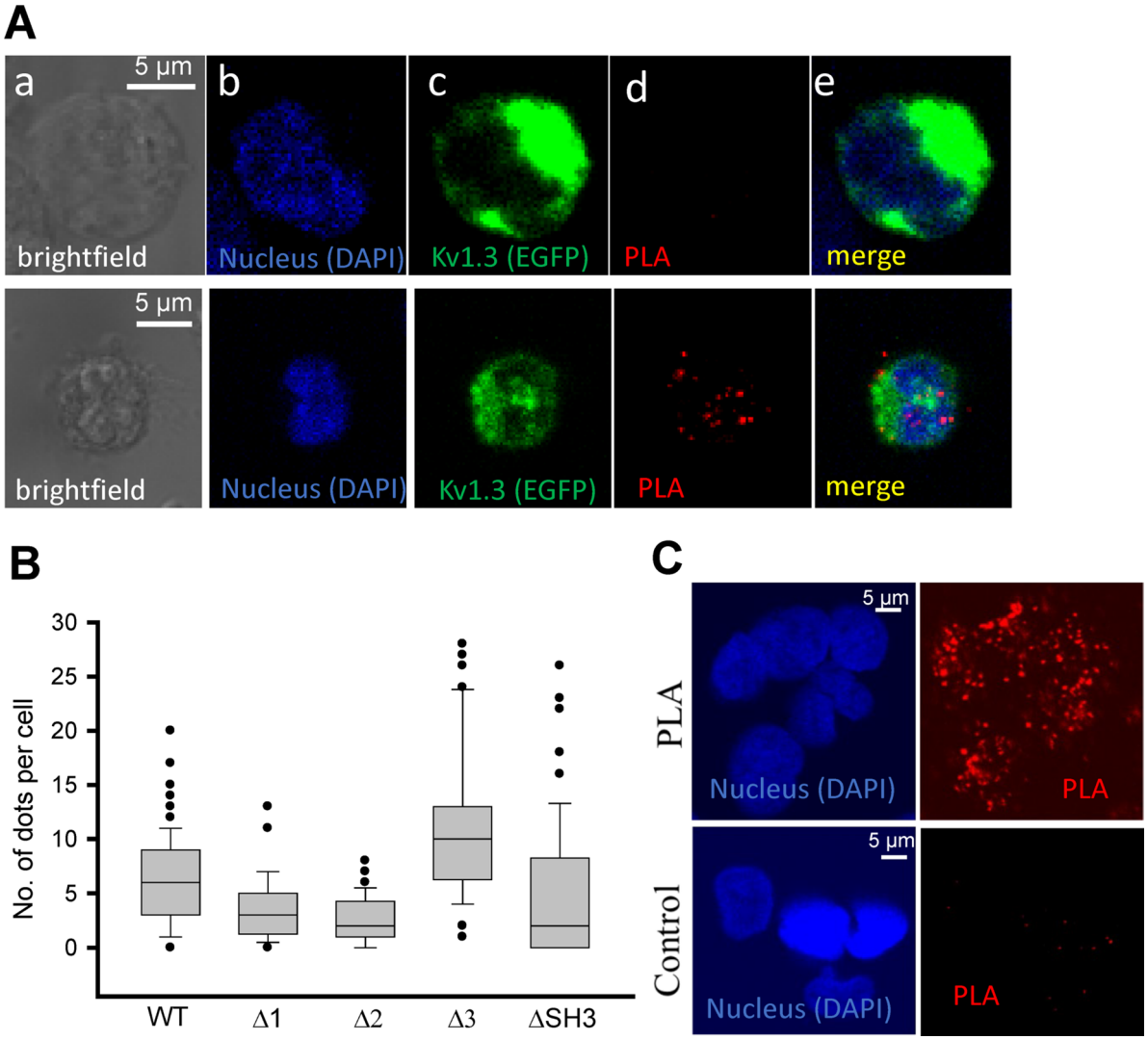

FIGURE 4: Cortactin and Kv1.3 channel interaction in HEK-293 cells. (A) PLA experiments performed with wild-type and EGFP-Kv1.3–transfected HEK-293 cells. Top, negative control: only secondary antibodies were added. Bottom, both primary (anti-GFP and anti-cortactin) and secondary antibodies were used. Single protein interactions are visualized as fluorescent red dots. (B) Box plot of number of PLA dots per cell. The data are reported as median, first (top box) and third quartiles (bottom box), and maximum and minimum of 93 cells for WT, 44 for Δ1, 34 for Δ2, 60 for Δ3, and 78 for ΔSH3. All the groups are significantly different from each other ($p < 0.001$), except for ΔSH3 vs. Δ2. (C) Interaction between actin and cortactin in HEK-293 cells. HEK-293 cells were labeled with (top) or without (bottom; only PLA antibodies) rabbit anti-human cortactin and mouse anti-human actin antibodies, and then PLA probe–ligated secondary antibodies were added and PLA was performed according to the manufacturer's protocol. Nuclear staining (4′,6-diamidino-2-phenylindole, blue) and PLA signal (red). Scale bar, 5 µm.

wild-type Kv1.3 channels in these cells lines and subjected them to FRAP experiments with or without jasplakinolide treatment (Figure 6B). The M_f of Kv1.3 channels in cortactin-knockdown cells was the same regardless of preincubation with jasplakinolide or not ($M_f = 0.61 \pm 0.03$ for control [$n = 5$] and 0.50 ± 0.08 for jasplakinolide [$n = 5$]; $p = 0.43$). On the contrary, the mobility of wild-type channels significantly dropped in control shRNA–transduced cells when actin stabilization was provoked by jasplakinolide ($M_f = 0.66 \pm 0.04$ for control [$n = 4$] and 0.41 ± 0.09 for jasplakinolide [$n = 4$], $p = 0.033$). These studies further confirm the role of cortactin in the F-actin–mediated lateral motility of Kv1.3.

Interaction of Kv1.3 and HS1 in T-lymphocytes

The studies reported so far demonstrated that an association exists between recombinant Kv1.3 channels and cortactin in HEK-293 cells. Further immunohistochemistry experiments in primary T-cells showed that native Kv1.3 channels and HS1 (the cortactin analogue expressed in T-cells) colocalize at the IS (Figure 7A). Primary human T-cells were activated with beads coated with anti–cluster of differentiation 3 (CD3) and anti-CD28 antibodies (CD3/CD28 beads). These beads mimic APCs: they bind to the T-cells, induce the formation of the IS, and activate them (Nicolaou *et al.*, 2007). Cells coupled with CD3/CD28 beads were stained for endogenous Kv1.3 (green) and HS1 (red). The merge image in Figure 7A shows colocalization of these two proteins at the bead/T-cell contact point (the IS). The actual interaction between Kv1.3 and HS1 at the IS was established by PLA experiments in Jurkat T-cells stably expressing GFP-tagged WT Kv1.3 channels (Figure 7, B and C). PLA-positive signal was present at the IS, where Kv1.3 accumulates (Supplemental Figure S2). On the contrary, when PLA was performed on cells that

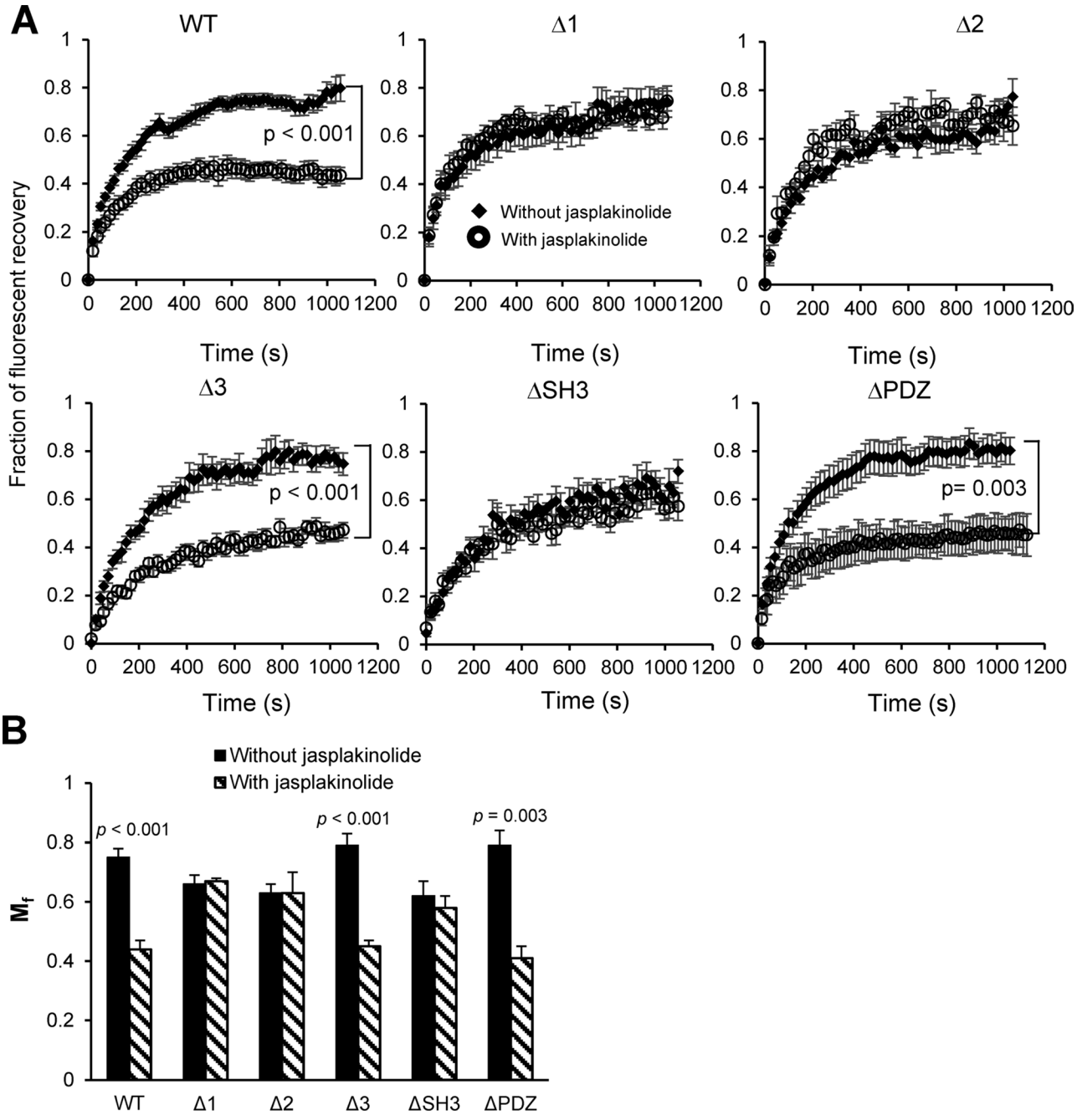

FIGURE 5: FRAP recovery curves of Kv1.3 wild-type and mutant channels. (A) Fraction of fluorescence signal recovery at each time point averaged over all FRAP experiments for each respective Kv1.3 channel type in HEK-293 cells. Curves depicted include experiments both without jasplakinolide pretreatment of HEK-293 cells (♦) and with jasplakinolide pretreatment (○). Error bars represent the SE of these averages at each time point (*n* without/with jasplakinolide: 7/7 for WT, 6/6 for Δ1, 7/3 for Δ2, 7/7 Δ3, 6/6 for ΔSH3. and 8/4 for ΔPDZ). (B) Average M_f for each individual mutant and WT Kv1.3. M_f differences with $p < 0.05$ between trials with and without jasplakinolide pretreatment are listed.

expressed truncated ΔC Kv1.3 channels (see also Figure 2C), although these channels are recruited at the IS, they do not interact with HS1, as indicated by the significant drop in the PLA signal (Figure 7, B and C). Similarly, WT Kv1.3 channels do not associate with HS1 in resting T-cells, which were not exposed to CD3/CD28 beads (no IS). These data indicate that Kv1.3–HS1 interaction occurs only upon activation of T-cells and strictly happens at the IS. Furthermore, they emphasize that HS1 in T-lymphocytes, like cortactin in HEK-293 cells, interacts with Kv1.3 via the carboxyl terminal of the channel.

DISCUSSION

As described by various groups, cortactin can bind to ion channels; however, the site of interaction is unresolved. An extensive study by Morielli's group described the 19–amino acid span on the C-terminus of the Kv1.2 channel as an essential element in the channel's

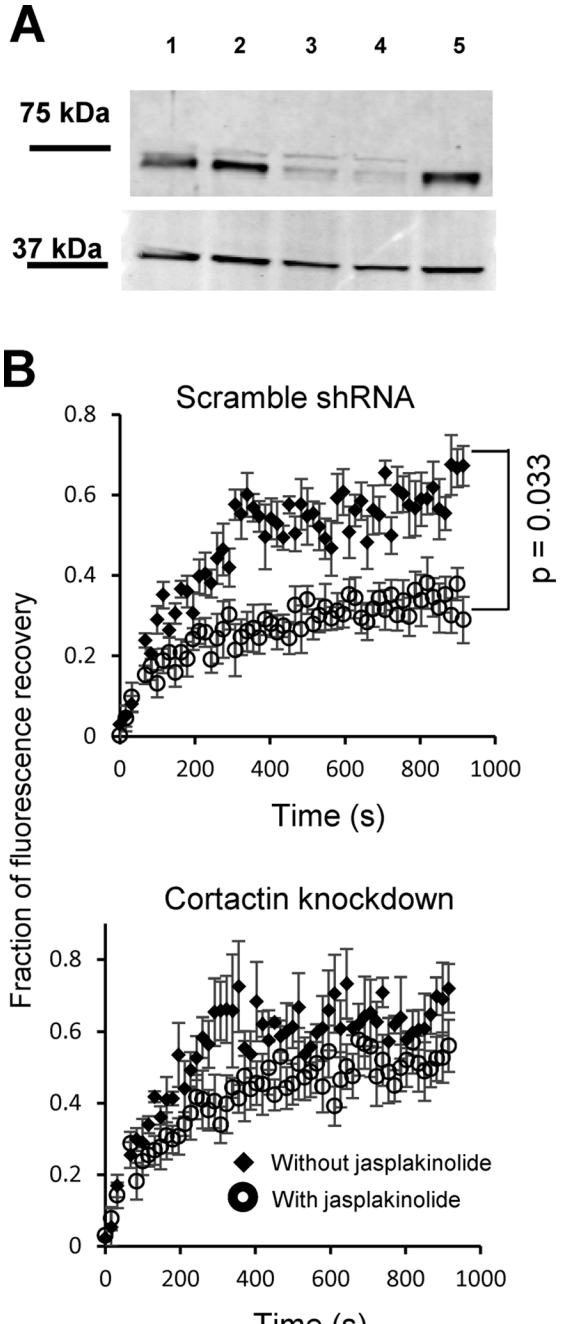

FIGURE 6: Cortactin-knockdown annuls the effect of jasplakinolide. (A) Western blot of total cell lysates of HEK-293 cells transduced with cortactin or scramble shRNA virus particles using cortactin antibody (1, 2: scramble shRNA; 3, 4: cortactin shRNA, 5: nontransduced HEK-293). A 20-μg amount of protein lysate was loaded in each lane, and the transferred proteins were probed with rabbit anti-cortactin antibody, with mouse anti–β-actin used as a loading control. (B) Averaged FRAP recovery curves of Kv1.3 wild-type channel in cortactin-altered HEK-293 cells. Fraction of fluorescence signal recovery at each time point averaged over all FRAP experiments for wild-type Kv1.3 channels with or without cortactin knockdown. Plotted curves include experiments without jasplakinolide pretreatment (♦) and with jasplakinolide pretreatment (○). Error bars represent the SE of these averages at each time point ($n = 4$ or 5). Mobile fraction differences with $p < 0.05$ between trials with and without jasplakinolide pretreatment are listed on the individual graphs.

coupling to cortactin (Williams *et al.*, 2007; Cheng *et al.*, 2011). Furthermore, this group also described that fusion of the SH3-binding domain with the truncated Kv1.2, which does not have the cortactin-binding site, can partially restore the coupling of cortactin to the channel (Hattan *et al.*, 2002; Williams *et al.*, 2007). Surprisingly, the phosphorylation of tyrosine residues upstream of the cortactin-binding domain of Kv1.2 abolished the interaction between the channel and cortactin (Hattan *et al.*, 2002; Williams *et al.*, 2007). Others showed that cortactin binds directly to the SH3-binding domains of the C-terminal region of the epithelial sodium channel (ENaC) and the large–conductance, Ca^{2+}-activated K channel (BKCa) without any adaptor proteins (Tian *et al.*, 2006; Ilatovskaya *et al.*, 2011). Here we demonstrated by means of the PLA that in an intact cell, the interaction between cortactin and Kv1.3 channels exclusively occurs through the SH3 domain, and the other potential binding sequences of the Kv1.3 have hardly any influence on this coupling. These data indicate that other cortactin-binding sites existing on the Kv1.3 protein are unavailable in an intact cell setting, where they may be masked by posttranslational modifications and/or the presence of other proteins that compete for those sites. Experiments with the ΔPDZ mutant showed that disruption of the PDZ-binding domain did not modify cortactin channel binding, which confirms the direct coupling between Kv1.3 and cortactin. This is in agreement with what was reported for other channels (Tian *et al.*, 2006; Ilatovskaya *et al.*, 2011). Further PLA experiments verified that the Kv1.3–HS1 interaction in Jurkat T-cells occurs via the C-terminus of the channel. Nevertheless, this coupling is not constitutive and triggered by TCR activation and intracellular mediators not yet known, as the PLA positivity was only seen in the IS-engaged but not standalone T-cells (Figure 7). Overall these results point to the existence of a physical association between cortactin (and HS1) and Kv1.3 and its possible role in cytoskeleton-regulated functions.

The functional studies reported here discovered a role for actin and cortactin in Kv1.3 membrane motility. The FRAP studies revealed that actin polymerization/remodeling induced by jasplakinolide can lead to a significant decrease in M_f of Kv1.3 channels, which were described to ramble more or less freely in the plasma membrane (O'Connell and Tamkun, 2005). Here we provide evidence for a role of the actin cytoskeleton in locking Kv1.3 and limiting its diffusion in the plasma membrane. Binding of PDZ proteins to Kv channels was shown to induce clustering of Kv1.3, Kv1.4, and Kv1.5 channels into cell surface domains and reduce Kv1.5 cell membrane mobility (Imamura *et al.*, 2002; Marks and Fadool, 2007). In our studies, PDZ-domain adaptor proteins such as hDlg and PSD-95 were excluded as regulators of Kv1.3 membrane motility (the M_f of the ΔPDZ mutant before actin polymerization is equivalent to that of WT channels) and as linkers of the cortical cytoskeleton and Kv1.3. By mutating the PDZ-binding domain (ΔPDZ), we could observe the same immobilization of the channels upon jasplakinolide treatment as observed in WT Kv1.3. Both Δ1 and Δ2 mutants instead showed no significant "arrest" by the induction of actin polymerization (Figure 5), indicating that the putative cortactin-binding site is insufficient to provide a functional attachment of Kv1.3 to the cytoskeleton. On "readdition" of SH3-binding site (Δ3), the drop in M_f after actin polymerization was comparable to that of wild-type channels. Conversely, mutation of the SH3-binding motif (ΔSH3) canceled the channel's immobilization by jasplakinolide. Overall these data support a model in which the interaction between cortactin and Kv1.3 has functional implications only when actin remodeling is induced. When no actin polymerization occurs, the channels presumably diffuse freely along the plane of the membrane, but upon actin polymerization,

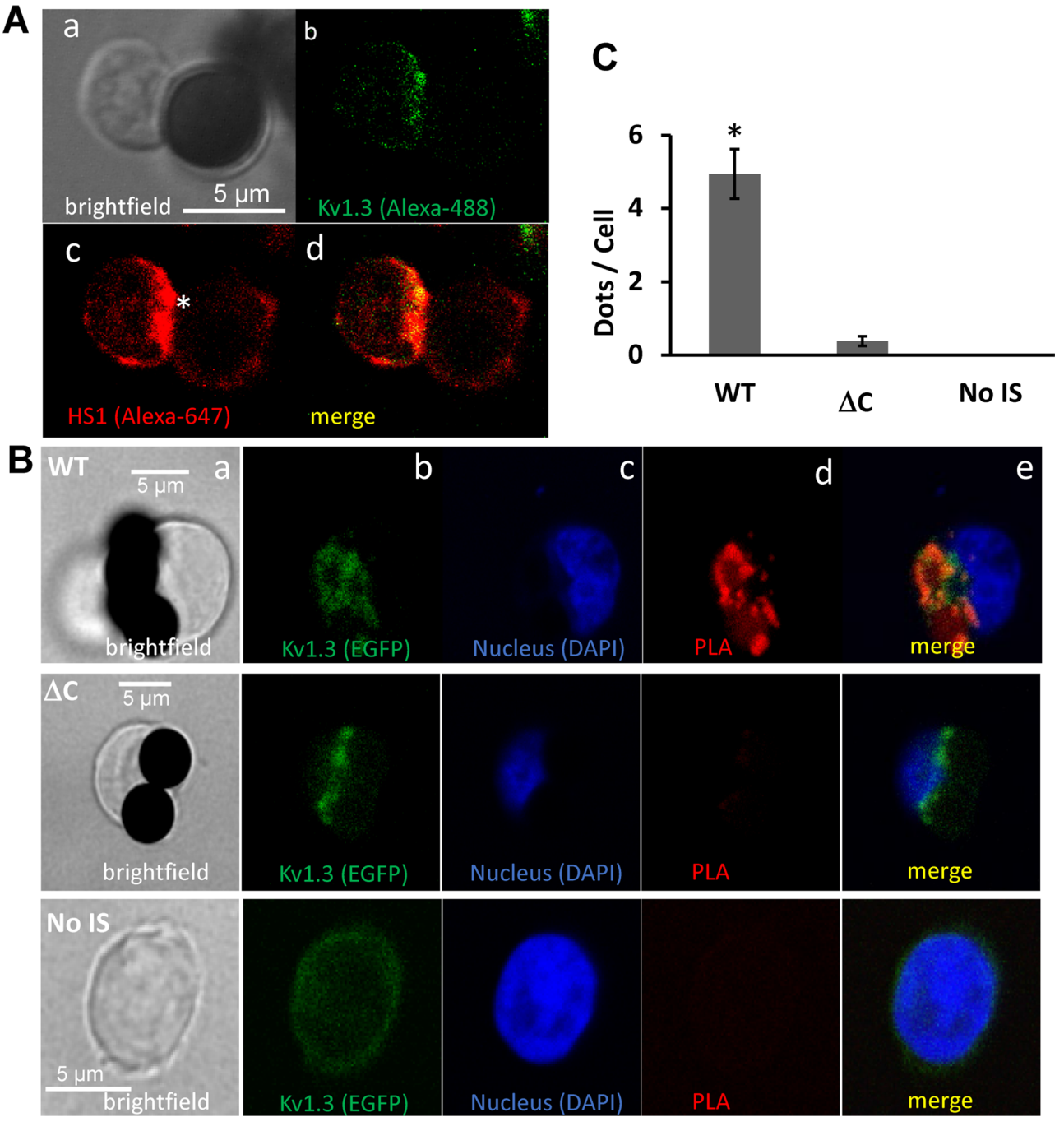

FIGURE 7: HS1 and Kv1.3 interact at the immunological synapse. (A) Micrographs (1-µm slice size) of human primary T-cells forming immunological synapses (denoted with an asterisk in c) with CD3/CD28 bead at 30 min. (a) Bright field, (b) Kv1.3 (green), (c) HS1 (red), (d) merge of green and red channels. Yellow denotes colocalization of Kv1.3 and HS1. (B) Confocal images of representative cells from PLA experiments performed in Jurkat cells stably expressing wild-type mGFP-Kv1.3 channels (WT, top) and mGFP-Kv1.3 channels with a C-terminal truncation (ΔC, middle) forming immunological synapses with CD3/CD28 beads at 30 min. Bottom, Jurkat cells overexpressing WT mGFP-Kv1.3 without beads (no IS). Single protein interactions are visualized as red fluorescence dots. (C) Average PLA signals. PLA signals were quantified in cells as number of dots per cell and are represented as mean ± SEM for 53 cells for WT, 86 for ΔC, and 91 for resting, no-IS cells. Statistically significant difference was observed in WT vs. ΔC and WT vs. no-IS groups ($p < 0.05$), whereas no significant difference was observed between the ΔC and no-IS groups.

the channel–cortactin complex becomes trapped by the F-actin network. Consequently, the SH3-binding motif provides the interface for cortactin–Kv1.3 coupling as reported for ENaC and BKCa and confirmed by the PLA results.

Cortactin has also been reported to regulate the surface expression of ion channels (Hattan *et al.*, 2002; Williams *et al.*, 2007; Cheng *et al.*, 2011; Herrmann *et al.*, 2012). By patch clamping, we found that all EGFP-tagged Kv1.3 mutant plasmids were expressed in

HEK-293 cells and could form conducting tetrameric channels. It was shown recently that two glutamic acids (E) at positions 483 and 484 of Kv1.3 carboxy-terminus are part of the cell membrane sorting sequence and aid forward trafficking (Martínez-Mármol *et al.*, 2013). Here we observed that their removal in the Δ1 construct did not influence the detection of EGFP signal in the plasma membrane. Nevertheless, we cannot exclude that Δ1 truncation leads to a lower expression level in the whole-cell configuration (here we used outside-out patches) and that assembly with endogenous Kv1.3 subunits in HEK-293 steered the heteromeric channels to the plasma membrane. Note that for our ΔC mutant, we did not obtain a different expression level in Jurkat T-cells than with the wild-type Kv1.3 (Szilagyi *et al.*, 2013). Hence we extrapolate the same to be true for all Kv1.3 constructs tested here. Because the channels were overexpressed in HEK-293 cells, a possible reduction in the mutant channel's targeting to the membrane had no effect on the measurement of Kv1.3 diffusion, as indicated by the similar values of baseline M_f (before jasplakinolide addition).

Finally, knockdown of cortactin clearly demonstrated that assemblage of F-actin with Kv1.3 channels is mediated by cortactin upon jasplakinolide stimulation. Wild-type Kv1.3 channels expressed in cortactin-silenced cells did not show immobilization by jasplakinolide treatment, unlike channels transfected into scramble shRNA–treated cell line (Figure 6B). Owing to the elimination of the linker element, Kv1.3 channels are not affixed to the cytoskeleton and, upon actin remodeling, can freely move in the plasma membrane. Hence cortactin has a pivotal role in the anchoring of Kv1.3 channels.

In this study, we showed that the pore-forming α subunit of another potassium ion channel is coupled to the cortical actin network, which stabilizes it upon F-actin nucleation. Because Kv1.3 channels are part of molecular machinery required for activation of T-cells, our results may provide new insights into the mechanisms that control Kv1.3 membrane localization in the IS, which is of great importance in T-cell function. The PLA experiments in T-cells showed that the lack of HS1-binding site does not preclude the channel from entering the IS, suggesting that HS1 may not affect Kv1.3 diffusion into the IS. Therefore it is possible that HS1 may alter the time Kv1.3 resides in the IS or its association with signaling molecules also residing at the IS that ultimately control its activity (Nicolaou *et al.*, 2010; Kuras *et al.*, 2012). However, these hypotheses should be tested to understand the functional significance of HS1–Kv1.3 interaction in T-cells. Overall the results presented here raise the possibility that the association between HS1 and Kv1.3 channels may shape the outcome of the signaling pathways during T-cell activation.

MATERIALS AND METHODS

Kv1.3 channel constructs

Plasmids (pEGFP-C1 backbone; Clontech, Mountain View, CA) containing EGFP-tagged WT and mutant Kv1.3 channels were generated for expression in HEK-293 cells. EGFP attachment to the N-terminus of Kv1.3 constructs was performed as previously described (Nicolaou *et al.*, 2010). C-terminal Kv1.3 mutants were generated by either amino acid sequence truncations or specific amino acid mutagenesis. Truncated C-terminal Kv1.3 mutants were created by insertion of a premature stop codon into the Kv1.3 DNA sequence before the specified truncation site. Truncation sites were specified just before the presumed cortactin binding site at amino acid 466 (Δ1 mutant), after the presumed cortactin-binding site at amino acid 487 (Δ2 mutant), and after an SH3-binding motif (-P-x-x-P-) at amino acid 496 (Δ3). The presumed cortactin-binding site of Kv1.3 was determined from the analogous amino acid sequence in Kv1.2 (Hattan *et al.*, 2002). A C-terminal mutant with altered SH3-binding motif (ΔSH3) was generated by changing proline residues at amino acids 493 and 496 to glycines, and a C-terminal mutant with altered PDZ-binding domain (ΔPDZ) was generated by changing the amino acid sequence FTDV at the end of the C-terminus to WSGG. Plasmid for the ΔSH3 mutant was a gift from D. A. Fadool (Florida State University, Tallahassee, FL) and has been previously described (Marks and Fadool, 2007). A schema of Kv1.3 wild type and C-terminal mutant can be found in Figure 2. We generated a construct for rat Kv1.3 containing a FLAG tag between D222 and V223 in the extracellular loop between S1 and S2 transmembrane domains. Briefly, a DNA fragment containing the nucleotide sequence corresponding to a FLAG tag (YKDDDDK) was generated by two-step overlapped PCR. The generated fragment was replaced with the corresponding portion of Kv1.3 cDNA using *Sph*I and *Pst*I sites. The sequence of the PCR-amplified portion was verified by DNA sequencing.

Cell culture and transfection

HEK-293 cells were cultured in DMEM (Fisher Scientific, Pittsburgh, PA) supplemented with 10% fetal bovine serum, 1 mM Na pyruvate, and 200 U penicillin/streptomycin (HEK-293 medium). HEK-293 cells stably expressing FLAG-tagged Kv1.3 channels or host plasmid (pcDNA3.1) were also grown in HEK-293 medium containing 1 mg/ml G418 (Sigma-Aldrich, St. Louis, MO). Transfections of DNA plasmids were done using Lipofectamine 2000 (Life Technologies, Carlsbad, CA) according to the manufacturer's protocol. For cortactin-knockdown experiments HEK-293 cells were transduced with lentivirus-based shRNA virus particles produced at the Lenti-shRNA Library Core, Cincinnati Children's Hospital (www.cincinnatichildrens.org/research/cores/lenti/default/). The protocol for viral infection and cell culturing (puromycin selection) is available at www.cincinnatichildrens.org/research/cores/lenti/background-protocol/. Briefly, HEK-293 cells were plated 24 h before lentiviral transduction in DMEM. The next day, the medium was replaced with fresh DMEM containing 10 μg/ml Polybrene (Sigma-Aldrich) and lentiviral supernatant, which contained virus particles with cortactin or negative control shRNAs (Mission shRNA; Sigma-Aldrich). Nontarget shRNA–containing virus particles were used as negative control. Knockdown cells were selected with 1–2 μg/ml puromycin (Sigma-Aldrich). The efficiency of knockdown was monitored with a Western blot technique.

Primary T-cells and Jurkat cells

Human T-cells were isolated from the blood of healthy consenting donors and discarded blood units from Hoxworth Blood Center (University of Cincinnati, Cincinnati, OH) using RosetteSep Human Total Lymphocyte Enrichment Cocktail (StemCell Technologies, Vancouver, Canada). The protocol was approved by the University of Cincinnati Institutional Review Board. T-cells were maintained in RPMI-1640 medium supplemented with 10% human serum, 200 U/ml penicillin, 200 μg/ml streptomycin, and 10 mM 4-(2-hydroxyethyl)-1-piperazineethanesulfonic acid (HEPES; T-cell medium). Jurkat E6-1 cells were maintained in RPMI-1640 medium with 10% human serum, 200 U/ml penicillin, 200 μg/ml streptomycin, and 10 mM HEPES and passed every other day.

Stable-transfected WT and ΔC Kv1.3 Jurkat T-cells were described previously (Szilagyi *et al.*, 2013).

Electrophysiology

HEK-293 cells transfected with various Kv1.3 channel constructs were washed with standard bath solution (composition [mM]: 145 NaCl, 5 KCl, 1 $MgCl_2$, 2.5 $CaCl_2$, 5.5 glucose, 10 HEPES) and

plated onto poly-L-lysine–coated glass coverslips. Kv1.3 currents were recorded in outside-out configuration using Axopatch 200B amplifier (Axon Instruments, Foster City, CA) as previously described (Szigligeti *et al.*, 2006). The pipette solution contained (mM) 140 KF, 11 K_2–ethylene glycol tetraacetic acid, 1 $CaCl_2$, 2 $MgCl_2$, and 10 HEPES (pH 7.20, ~295 mOsm). A P/5 protocol for online leaks subtraction was applied to minimize capacitance and leak errors during the determination of the activation kinetics.

The inactivation kinetics of each construct was determined by fitting a single- exponential function ($I(t) = I_0 \exp(-t/\tau_i) + C$, where I_0 is the amplitude of the current, τ_i is the inactivation time constant, and C is the steady-state value of whole-cell current at the end of the pulse) to the decaying part of the traces evoked by 2-s-long depolarization to +40 mV from a holding potential (HP) of –120 mV.

The voltage dependence of steady-state activation was determined as follows. The outside-out patches were clamped at –120 mV HP, and depolarizing test potentials from –70 to +50 mV were delivered in 10-mV steps every 30 s. Peak conductance ($G(V)$) at each test potential was calculated from the peak current (I_p) at test potential (V) and the K^+ reversal potential ($E_r = -85$ mV) from the equation $G(V) = I_p/(V - E_r)$. The $G(V)$ values were normalized for the maximum conductance and plotted against the test potential. A Boltzmann function was fitted to the data points: $G_N = 1/\{1 + \exp[-(V - V_{1/2})/k]\}$, where G_N is the normalized conductance, V is the test potential, $V_{1/2}$ is the midpoint, and k is the slope of the function.

Immunocytochemistry

HEK-293 cells stably expressing FLAG-Kv1.3–encoding plasmid or empty vector (pcDNA3.1; Life Technologies) were plated onto poly-L-lysine coverslips and incubated for 3–4 h (37°C, humidified, 5% CO_2). Then cells were fixed with 1% formaldehyde and labeled with rabbit anti-FLAG antibody (10 µg/ml; Sigma-Aldrich) overnight at 4°C. Afterward, cells were permeabilized with 0.2% Triton X-100 for 20 min at room temperature, and mouse anti-cortactin antibody (1:50 dilution; Santa Cruz Biotechnology, Dallas, TX) was added overnight at 4°C. Secondary antibodies (donkey anti-rabbit with Alexa 488, goat anti-mouse with Alexa 647; Life Technologies) were added to the cells for 1 h at room temperature. Finally, coverslips were mounted onto slides with Fluoromount G (eBioScience, San Diego, CA). A Zeiss LSM 510 META microscope (Carl Zeiss Microscopy GmbH) was used to take confocal images of the cells (63× oil immersion lens, numerical aperture [NA] 1.4). A HeNe laser was selected to excite fluorophore Alexa 647 (633-nm line) and an argon laser (488-nm line) to visualize Alexa 488. The thickness of the slices and *z*-stacks was set to 1 µm.

Immunological synapses were formed between either resting T-lymphocytes or Jurkat T-cells and anti-CD3/anti-CD28 antibody (CD3/CD28)–coated polystyrene beads (Life Technologies) as detailed earlier (Nicolaou *et al.*, 2007). Cell–bead conjugates were fixed 5 and 30 min after synapse formation and labeled with rabbit anti-Kv1.3 antibody (Alomone, Israel) at 4°C overnight. Then the cells were permeabilized as described for HEK-293 cells, and goat anti-HS1 antibody (R&D Systems, Minneapolis, MN) was added. The secondary antibodies (goat anti-rabbit immunoglobulin G A488, donkey anti-goat A647; Life Technologies) were incubated for 1 h at room temperature. Afterward, coverslips were mounted onto slides with Fluoromount G. The confocal snapshots were taken as described. For a detailed description of immunological synapse quantification see Supplemental Information 2 and Supplemental Figure S2.

Western blotting

For shRNA experiments, transfected HEK-293 cells were lysed using Pierce IP Lysis Buffer along with HALT Protease Inhibitor cocktail (ThermoFisher Scientific, Waltham, MA) as previously described (Chimote *et al.*, 2012). The protein content of the lysates was measured using the BCA Protein Assay (ThermoFisher Scientific). Cell lysates were mixed with 3× SDS sample buffer (New England Biolabs, Ipswich, MA), and 20 µg of protein was loaded on to each lane of a 4–12% Tris-glycine gel (Life Technologies) in an X Cell SureLock Gel System (Life Technologies). The protein bands were transferred to a polyvinylidene fluoride membrane (Life Technologies) in an X Cell II Blot Module (Life Technologies). The membrane was blocked with Odyssey Blocking Buffer (LI-COR Biosciences, Lincoln, NE) at room temperature for 1 h and subsequently incubated overnight at 4°C with a polyclonal rabbit antibody against cortactin (Santa Cruz Biotechnology) along with a mouse monoclonal antibody against β-actin (Alpha Diagnostic International, San Antonio, TX). The blot was thoroughly washed with phosphate-buffered saline/Tween and incubated with Alexa Fluor 680 anti-rabbit and IRDye 800CW anti-mouse secondary antibodies for 60 min at room temperature (Life Technologies). The blots were then visualized with the LI-COR Odyssey infrared scanner at 169-µm resolution.

Proximity ligation assay

PLA experiments were performed using Duolink In Situ PLA Kit (Sigma-Aldrich) with Detection Reagents Red as suggested by the manufacturer's protocol. HEK-293 cells were transfected with EGFP-tagged Kv1.3 constructs, then plated onto poly-L-lysine–coated coverslips. Primary antibodies were mouse anti-GFP (1:200; Miltenyi Biotec, San Diego, CA) and rabbit anti-cortactin (1:200; Santa Cruz Biotechnology). Jurkat cells stably expressing GFP-WT or ΔC Kv1.3 channels were incubated with CD3/CD28 beads for 30 min and plated on poly-L-lysine– coated coverslips. Cells incubated without the beads were used as controls (resting, no IS, T-cells). Cells were fixed permeabilized and then incubated with mouse anti-GFP (1:200; Miltenyi Biotec) and goat anti-HS1 (1:200; R&D systems). Confocal images were taken with a Zeiss LSM 710 microscope with 63× water immersion lens (pinhole was set to 1 Airy unit). Individual interacting molecule pairs are detected as bright fluorescent spots. Evaluation of PLA snapshots was done by the Duolink Image Tool software (demo version), which allows quantitating the PLA signal.

Fluorescence recovery after photobleaching

Transfected HEK-293 cells were plated onto collagen and poly-L-lysine–coated glass coverslips and incubated in DMEM without phenol red at 37°C for at least 1 h before performing FRAP experiments. Cells were also bathed in DMEM without phenol red during FRAP measurements. A subset of cell coverslips was also bathed in a solution containing the actin-polymerizing agent jasplakinolide (Calbiochem, San Diego, CA; 2 µM; dimethyl sulfoxide 1:1000 dilution in control cells) for 50 min at 37°C before FRAP measurements. FRAP experiments were performed on a Zeiss LSM 510 Meta confocal microscope with a 40× water immersion objective (NA 1.2) at room temperature. Pinhole size was set between 0.8 and 0.86 µm (slice thickness, ~1 µm). During the measurements, EGFP-tagged Kv1.3 channels were excited with a 488-nm argon laser that was passed through an EGFP filter of 505–535 nm at 1% power for prebleach and postbleach measurements. Photobleaching was confined to a region of interest (ROI) along the cell membrane and performed with the argon laser (488 nm) at 100% power for 100 bleach iterations over this ROI. Confocal images during FRAP

experiments were acquired every 15 s at a resolution of 512 × 512 and 3× zoom for a total of 60 scans. The background fluorescence was subtracted from the average fluorescence intensity over the photobleached ROI from each image and then normalized to the prebleach intensity. These normalized values were used for the final analysis. The mobile fraction (M_f) was determined using

$$M_f = \frac{F_\infty - F_0}{F_i - F_0} \quad (1)$$

where F_∞ is the fluorescence at the end of the FRAP experiments, F_0 is the fluorescence intensity immediately postbleach, and F_i is the fluorescence prebleach.

Coimmunoprecipitation experiments

Technical details and protocol for Kv13.-hDlg coimmunoprecipitation experiments are described in Supplemental Information 1.

Statistical analysis

Data are expressed as the mean ± SE. Means were compared using Student's *t* test, one-way analysis of variance (ANOVA), and one-way ANOVA on ranks. $p < 0.05$ was considered statistically significant. Statistical analyses were performed using SPSS version 21.0 (IBM, Armonk, NY).

ACKNOWLEDGMENTS

We greatly appreciate the technical assistance of Lisa Neumeier and Charles Ebersbacher. This project was funded in part by American Heart Association Grant-in-Aid 0855457D and National Institutes of Health Grant R01CA095286. O.S. was supported by the European Union and the state of Hungary, cofinanced by the European Social Fund in the framework of the TÁMOP 4.2.4. A/2-11-1-2012-0001 National Excellence Program. This project was partly supported by the Hungarian Social Renewal Operational Program (TAMOP-4.2.2-A-11/1/KONV-2012-0025).

REFERENCES

Babich A, Li S, O'Connor RS, Milone MC, Freedman BD, Burkhardt JK (2012). F-actin polymerization and retrograde flow drive sustained PLCgamma1 signaling during T cell activation. J Cell Biol 197, 775–787.

Bubb MR, Senderowicz AM, Sausville EA, Duncan KL, Korn ED (1994). Jasplakinolide, a cytotoxic natural product, induces actin polymerization and competitively inhibits the binding of phalloidin to F-actin. J Biol Chem 269, 14869–14871.

Bubb MR, Spector I, Beyer BB, Fosen KM (2000). Effects of jasplakinolide on the kinetics of actin polymerization. An explanation for certain in vivo observations. J Biol Chem 275, 5163–5170.

Cahalan MD, Chandy KG (2009). The functional network of ion channels in T lymphocytes. Immunol Rev 231, 59–87.

Carrizosa E, Gomez TS, Labno CM, Klos Dehring DA, Liu X, Freedman BD, Billadeau DD, Burkhardt JK (2009). Hematopoietic lineage cell-specific protein 1 is recruited to the immunological synapse by IL-2-inducible T cell kinase and regulates phospholipase Cγ1 microcluster dynamics during T cell spreading. J Immunol 183, 7352–7361.

Cheng L, Yung A, Covarrubias M, Radice GL (2011). Cortactin is required for N-cadherin regulation of Kv1.5 channel function. J Biol Chem 286, 20478–20489.

Chimote AA, Kuras Z, Conforti L (2012). Disruption of kv1.3 channel forward vesicular trafficking by hypoxia in human T lymphocytes. J Biol Chem 287, 2055–2067.

Daly RJ (2004). Cortactin signalling and dynamic actin networks. Biochem J 382, 13–25.

Davis SJ, van der Merwe PA (2006). The kinetic-segregation model: TCR triggering and beyond. Nat Immunol 7, 803–809.

Doczi MA, Damon DH, Morielli AD (2011). A C-terminal PDZ binding domain modulates the function and localization of Kv1.3 channels. Exp Cell Res 317, 2333–2341.

Douglass AD, Vale RD (2005). Single-molecule microscopy reveals plasma membrane microdomains created by protein-protein networks that exclude or trap signaling molecules in T cells. Cell 121, 937–950.

Dushek O, Mueller S, Soubies S, Depoil D, Caramalho I, Coombs D, Valitutti S (2008). Effects of intracellular calcium and actin cytoskeleton on TCR mobility measured by fluorescence recovery. PLoS One 3, e3913.

Dustin ML (2007). Cell adhesion molecules and actin cytoskeleton at immune synapses and kinapses. Curr Opin Cell Biol 19, 529–533.

Favier B, Burroughs NJ, Wedderburn L, Valitutti S (2001). TCR dynamics on the surface of living T cells. Int Immunol 13, 1525–1532.

Gomez TS, McCarney SD, Carrizosa E, Labno CM, Comiskey EO, Nolz JC, Zhu P, Freedman BD, Clark MR, Rawlings DJ, *et al.* (2006). HS1 functions as an essential actin-regulatory adaptor protein at the immune synapse. Immunity 24, 741–752.

Hajdu P, Chimote AA, Thompson TH, Koo Y, Yun Y, Conforti L (2013). Functionalized liposomes loaded with siRNAs targeting ion channels in effector memory T cells as a potential therapy for autoimmunity. Biomaterials 34, 10249–10257.

Hattan D, Nesti E, Cachero TG, Morielli AD (2002). Tyrosine phosphorylation of Kv1.2 modulates its interaction with the actin-binding protein cortactin. J Biol Chem 277, 38596–38606.

Herrmann S, Ninkovic M, Kohl T, Lörinczi É, Pardo LA (2012). Cortactin controls surface expression of the voltage-gated potassium channel KV10.1. J Biol Chem 287, 44151–44163.

Hu L, Wang T, Gocke AR, Nath A, Zhang H, Margolick JB, Whartenby KA, Calabresi PA (2013). Blockade of Kv1.3 potassium channels inhibits differentiation and granzyme B secretion of human CD8+ T effector memory lymphocytes. PLoS One 8, e54267.

Ilatovskaya DV, Pavlov TS, Levchenko V, Negulyaev YA, Staruschenko A (2011). Cortical actin binding protein cortactin mediates ENaC activity via Arp2/3 complex. FASEB J 25, 2688–2699.

Imamura F, Maeda S, Doi T, Fujiyoshi Y (2002). Ligand binding of the second PDZ domain regulates clustering of PSD-95 with the Kv1.4 potassium channel. J Biol Chem 277, 3640–3646.

Kummerow C, Junker C, Kruse K, Rieger H, Quintana A, Hoth M (2009). The immunological synapse controls local and global calcium signals in T lymphocytes. Immunol Rev 231, 132–147.

Kuras Z, Yun YH, Chimote AA, Neumeier L, Conforti L (2012). KCa3.1 and TRPM7 channels at the uropod regulate migration of activated human T cells. PLoS One 7, e43859.

Marks DR, Fadool DA (2007). Post-synaptic density perturbs insulin-induced Kv1.3 channel modulation via a clustering mechanism involving the SH3 domain. J Neurochem 103, 1608–1627.

Martínez-Mármol R, Pérez-Verdaguer M, Roig SR, Vallejo-Gracia A, Gotsi P, Serrano-Albarrás A, Bahamonde MI, Ferrer-Montiel A, Fernández-Ballester G, Comes N, Felipe A (2013). A non-canonical di-acidic signal at the C-terminus of Kv1.3 determines anterograde trafficking and surface expression. J Cell Sci 126, 5681–5691.

Mossman KD, Campi G, Groves JT, Dustin ML (2005). Altered TCR signaling from geometrically repatterned immunological synapses. Science 310, 1191–1193.

Nicolaou SA, Neumeier L, Steckly A, Kucher V, Takimoto K, Conforti L (2009). Localization of Kv1.3 channels in the immunological synapse modulates the calcium response to antigen stimulation in T lymphocytes. J Immunol 183, 6296–6302.

Nicolaou SA, Neumeier L, Takimoto K, Lee SM, Duncan HJ, Kant SK, Mongey AB, Filipovich AH, Conforti L (2010). Differential calcium signaling and Kv1.3 trafficking to the immunological synapse in systemic lupus erythematosus. Cell Calcium 47, 19–28.

Nicolaou SA, Szigligeti P, Neumeier L, Lee SM, Duncan HJ, Kant SK, Mongey AB, Filipovich AH, Conforti L (2007). Altered dynamics of Kv1.3 channel compartmentalization in the immunological synapse in systemic lupus erythematosus. J Immunol 179, 346–356.

O'Connell KM, Tamkun MM (2005). Targeting of voltage-gated potassium channel isoforms to distinct cell surface microdomains. J Cell Sci 118, 2155–2166.

Shin H, Hsueh Y-P, Yang F-C, Kim E, Sheng M (2000). An intramolecular interaction between Src homology 3 domain and guanylate kinase-like domain required for channel clustering by postsynaptic density-95/SAP90. J Neurosci 20, 3580–3587.

Soderberg O, Gullberg M, Jarvius M, Ridderstrale K, Leuchowius K-J, Jarvius J, Wester K, Hydbring P, Bahram F, Larsson L-G, Landegren U (2006). Direct observation of individual endogenous protein complexes in situ by proximity ligation. Nat Methods 3, 995–1000.

Szigligeti P, Neumeier L, Duke E, Chougnet C, Takimoto K, Lee SM, Filipovich AH, Conforti L (2006). Signalling during hypoxia in human T lymphocytes–critical role of the src protein tyrosine kinase p56Lck in the O2 sensitivity of Kv1.3 channels. J Physiol 573, 357–370.

Szilagyi O, Boratko A, Panyi G, Hajdu P (2013). The role of PSD-95 in the re-arrangement of Kv1.3 channels to the immunological synapse. Pflugers Arch 465, 1341–1353.

Tian L, Chen L, McClafferty H, Sailer CA, Ruth P, Knaus HG, Shipston MJ (2006). A noncanonical SH3 domain binding motif links BK channels to the actin cytoskeleton via the SH3 adapter cortactin. FASEB J 20, 2588–2590.

Williams MR, Markey JC, Doczi MA, Morielli AD (2007). An essential role for cortactin in the modulation of the potassium channel Kv1.2. Proc Natl Acad Sci USA 104, 17412–17417.

Wulff H, Calabresi PA, Allie R, Yun S, Pennington M, Beeton C, Chandy KG (2003). The voltage-gated Kv1.3 K(+) channel in effector memory T cells as new target for MS. J Clin Invest 111, 1703–1713.

Xavier R, Rabizadeh S, Ishiguro K, Andre N, Ortiz JB, Wachtel H, Morris DG, Lopez-Ilasaca M, Shaw AC, Swat W, Seed B (2004). Discs large (Dlg1) complexes in lymphocyte activation. J Cell Biol 166, 173–178.

Zhu J, Gomez B, Watanabe I, Thornhill WB (2007). Kv1 potassium channel C-terminus constant HRETE region: arginine substitution affects surface protein level and conductance level of subfamily members differentially. Mol Membr Biol 24, 194–205.

Zhu J, Watanabe I, Gomez B, Thornhill WB (2003). Trafficking of Kv1.4 potassium channels: interdependence of a pore region determinant and a cytoplasmic C-terminal VXXSL determinant in regulating cell-surface trafficking. Biochem J 375, 761–768.